UNIVERSITY OF HELSINKI

https://helda.helsinki.fi

Molecular dynamics simulation of the effects of swift heavy ion irradiation on multilayer graphene and diamond-like carbon

Liu, Jian; Muinos, Henrique Vazquez; Nordlund, Kai; Djurabekova, Flyura

2020-10-15
Elsevier B.V.
http://hdl.handle.net/10138/319459
Liu, J, Muinos, H V, Nordlund, K & Djurabekova, F 2020, 'Molecular dynamics simulation of the effects of swift heavy ion irradiation on multilayer graphene and diamond-like carbon', Applied Surface Science, vol. 527, 146495. https://doi.org/10.1016/j.apsusc.2020.146495

Downloaded from Helda, University of Helsinki institutional repository. https://helda.helsinki.fi
This is an electronic reprint of the original article.
This reprint may differ from the original in pagination and typographic detail.
Please cite the original version.

Published in:Applied Surface Science
Volume 527, 15 October 2020, 146495

Molecular Dynamics Simulation of the Effects of Swift Heavy Ion Irradiation on Multilayer Graphene and Diamond-Like Carbon

Jian Liu[a,b], Henrique Vázquez Muíños[a], Kai Nordlund[a], Flyura Djurabekova[a,*]

[a]*Helsinki Institute of Physics and Department of Physics, University of Helsinki, POB 43, 00014, Helsinki, Finland*
[b]*Department of Nuclear Science and Technology, Nanjing University of Aeronautics and Astronautics, Nanjing 210016, China*

Abstract

As a promising material used in accelerators and in space in the future, it is important to study the property and structural changes of graphene and diamond-like carbon on the surface as a protective layer before and after swift heavy ion irradiation, although this layer could have a loose structure due to the intrinsic sp^2 surrounding environment of graphene during its deposition period. In this study, by utilizing inelastic thermal spike model and molecular dynamics, we simulated swift heavy ion irradiation and examined the track radius in the vertical direction, as well as temperature, density, and sp^3 fraction distribution along the radius from the irradiation center at different time after irradiation. The temperature in the irradiation center can reach over 11000 K at the beginning of irradiation while there would be a low density and sp^3 fraction area left in the central region after 100 ps. Ring analysis also demonstrated a more chaotic cylindrical region in the center after irradiation. After comprehensive consideration, diamond-like carbon deposited by 70 eV carbon bombardment provided the best protection.

Keywords: Multilayer graphene, Diamond-like carbon, Inelastic thermal spike model, Molecular dynamics

*Corresponding author. E-mail: flyura.djurabekova@helsinki.fi (Flyura Djurabekova)

1. Introduction

Graphene is a stable 2D material that has numerous unique properties, such as ultra-high strength, electron mobility, and thermal conductivity, making it a desirable nanomaterial for many different applications. Graphene can be utilized as key components in field-emission transistors [1], biosensors [2], gas sensors [3], photovoltaic cells [4], transparent electrodes [5], and conductive films [6]. Graphene is also a promising material with low secondary electron emission for space application and large particle accelerators [7]. Despite these remarkable properties and wide applications, graphene still presents several drawbacks, such as high cost to grow and separate into mono- or bi-layers, frangibility to resist external damage, and high chemical activity to adsorb impurity atoms. Among all these weaknesses, the frangibility is the most severe hindrance that every graphene-based functional device will encounter during the manufacture and usage. Hence, many efforts have been exerted into finding a feasible way to protect graphene against scratch and wear. One effective solution is to cover graphene with diamond-like carbon (DLC), a metastable amorphous structure containing a wide range of sp^3 fraction and having a good reputation as an ideal protective material for nanostructures as well as enhancing mechanical strength of nanomaterials [8–10]. DLC not only has high hardness and elastic modulus [11], but also owns properties like transparency in the IR wavelength band [12] and chemical inertness [13], making it a hard shield against external damage while maintaining the original graphene structure with perfect electrical and thermal properties.

Humans have unquenchable desire to explore the outer space with the development of modern technology of space stations, space shuttles, and artificial satellites. Besides, a large amount of accelerator facilities are already in use and the number of more powerful and advanced accelerators for construction has increased with the development of modern accelerator technologies. This ensures that the swift heavy ion (SHI) beam generated from the accelerator can be controlled and continuously provided. Whether it is used in space or accelerators, graphene-based functional materials protected by DLC are promising for their intrinsic quality compared to conventional materials. Nevertheless, harsh environments consisting of various kinds of SHIs with energy ranging from several to hundreds of MeV are encountered in space applications and accelerators. Therefore, studying the structure modification and defects evolution of graphene and DLC after SHIs bombardment is

necessary, as well as the relevant mechanisms.

Experiments and simulations have shown that graphene and DLC exhibit some unique phenomena with regard to structure evolution and property changes. Schwen *et al.* studied field emission effects on SHI irradiated amorphous carbon with atomic force microscopy [14]. Zeng *et al.* used Raman spectroscopy to study SHI irradiation effects on monolayer graphene and highly oriented pyrolytic graphite [15]. Ochedowski *et al.* conducted experiments and revealed the radiation hardness of graphene field effect devices against SHI irradiation [16]. In simulation, inelastic thermal spike (i-TS) model [17] has been well established and developed to investigate the interaction between SHIs and target material atoms. Applied in simulations, i-TS model offers effective help in explaining a series of SHI irradiation phenomena. Vázquez *et al.* determined the threshold of electronic stopping power to form a defect and the relationship between stopping power and the diameter of defects [18]. Ren *et al.* studied the graphitization of carbon nanotubes embedded in DLC after incident SHI damaged the original structure [19]. Kupka *et al.* investigated the formation of 5- and 7-element carbon rings after the interaction between SHI and DLC [20]. Although the effects of SHIs on graphene and DLC have been widely investigated, there are still some problems that have to be resolved. Previous studies focused on monolayer graphene and DLC with dense structure, which is usually an ideal situation. Production of monolayer graphene is very difficult and expensive due to its extremely high surface energy, and monolayer graphene easily aggregates to form multilayer graphene. Meanwhile, DLC may contain relatively low sp^3 fraction and form loose structure on top of graphene, which needs to be protected, during the deposition process because graphene matrix is made up of sp^2 hybridized carbon and it is tough to grow sp^3 structure with sp^2 surroundings, according to our pervious study [21]. Thus, it will be more realistic to investigate the structure evolution and its mechanism after bombardment of incident SHIs on multilayer graphene and protective DLC with low sp^3 fraction.

In this study, we utilized i-TS model and molecular dynamics (MD) to study the structure evolution and related properties of multilayer graphene and low sp^3 fraction DLC after SHI irradiation. In addition, the intrinsic mechanism behind all the phenomena was also analyzed.

2. Simulation model and method

2.1. DLC deposition

To generate a DLC film with a loose structure, we first deposited DLC on top of a multilayer graphene. In the original structure, as shown in Figure 1, the six-layered graphene with the length 35 Å, the width 30 Å and the height 16.75 Å, was built of 2304 carbon atoms and placed on top of the diamond substrate with the length and width the same as of the graphene but the height of about 20 Å. The number of carbon atoms in diamond was 3456. The interlayer distance in multilayer graphene as well as the distance between diamond and the graphene were 3.35 Å, which is the interlayer distance in graphite according to many previous studies [22–24]. The two bottom layers of atoms in diamond were fixed to avoid downward movement of the whole structure due to incident momentum. Periodic boundaries were set for planar x- and y-directions, leaving vertical z-direction with non-periodic condition. The ambient temperature during the deposition runs was set to 100 K for better quality of DLC [21, 25]. Three incident energies, 50, 70, and 100 eV, were used separately. A carbon atom with a specific energy was placed at 5 Å above the surface and in the lateral center of the structure. After the atom sank into graphene, the whole structure relaxed for 10 ps to relax the stress generated due to the impact and cool down the entire system. Before introducing a subsequent carbon ion, the structure was laterally shifted by the radius with the x and y coordinates randomly chosen between zero and the length of the half-box in the corresponding direction. This procedure ensured the randomness of the incoming ion impacts on the surface, although the initial position of the ion could remain the same in all simulation runs. Then, the bombardment and relaxation process was repeated for around 8000 times. The Berendsen thermostat [26] method was also applied to graphene atoms within 5 Å from the cell borders to control the system temperature and prevent overheating after the bombardment. As a result of these simulations, the DLC film was formed with thickness of $\approx$ 55 Å. More detail on how the DLC films were built can be found elsewhere [21]. The deposition and later SHI irradiation were all simulated in classical molecular dynamics (MD) code PARCAS [27, 28], where Brenner-Beardmore potential [29–31] with extended cutoff R = 1.95 Å and S = 2.25 Å was applied to provide more sp^3 hybridized carbon atoms and more accurate results according to Jäger and Albe [32]. Although some other potentials like EDIP and COMB3 can lead to higher density in DLC [33, 34], they are more than 10 times slower to for simulations

of the same DLC structure with ~ 1 million atoms. Also different from liquid quenching method used in other works, in our work, we used direct energetic carbon atom deposition to create DLC film on top of multilayer graphene, to emulate the DLC deposition process in experiments and industries. Although this would lead to relatively low density, our method is more feasible in application. All visualized simulation structures in this study were obtained using the open visualization tool OVITO [35].

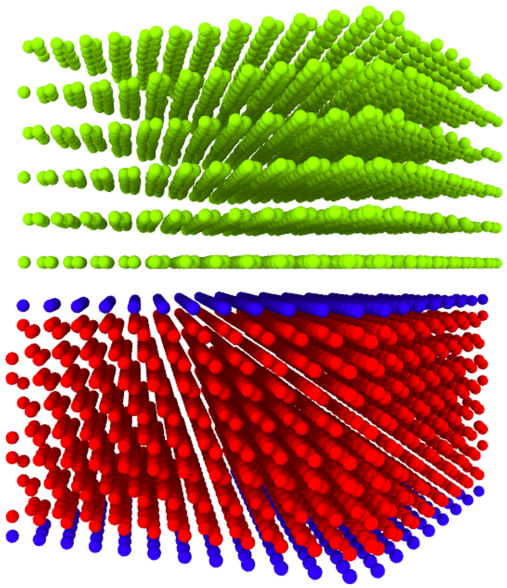

Figure 1: Diagrammatic representation of original model. Atoms are colored according to their coordination number, dark blue for 1, green for 3, and red for 4.

After the DLC deposition, the graphene was partially damaged and the remaining intact graphene layers decreased more with increase of incident energies from 50 to 100 eV. The fraction of sp^3 carbon atoms in DLC is 15.45%, 16.68%, and 10.42% corresponding to Figures 2(a), (b), and (c), respectively. Compared with the previous results [19, 20], the DLC structure in the present study is relatively loose and with lower density.

The built DLC-graphene-diamond structure was replicated 8 times along both x- and y-direction to form a large sandwich structure with size of about $270\times240\times100$ Å^3, as shown in Figures 2(a) to (c). This large size structures were used to enable the realistic evolution dynamics of the energy profile introduced by a passing swift heavy ion. During the SHI irradiation, ambient

temperature was set at the room temperature of 300 K.

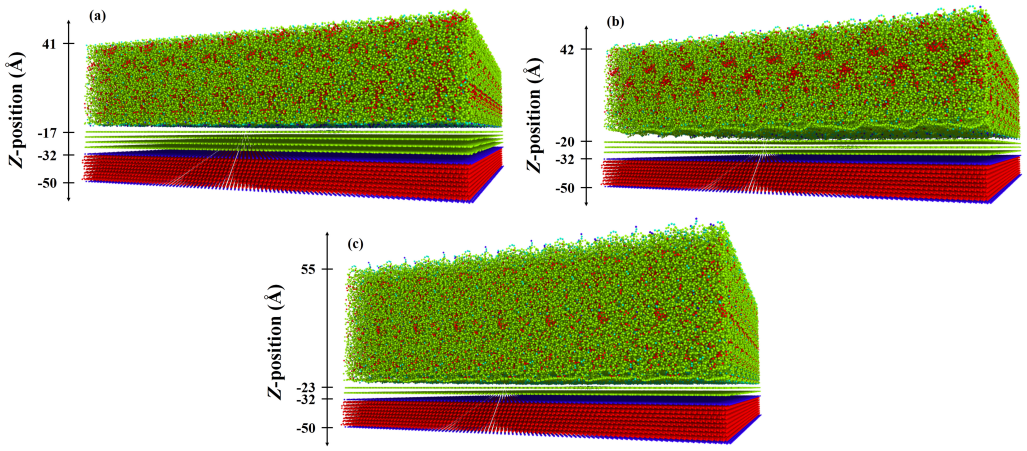

Figure 2: Representation of replicated DLC-graphene-diamond model corresponding to incident energies of (a) 50, (b) 70, and (c) 100 eV. Atoms are colored according to their coordination number: dark blue for 1, light blue for 2, green for 3, and red for 4.

2.2. Simulation setup for SHI irradiation

To simulate the impact of a 91 MeV Xe^{23+} ion with $(\frac{dE}{dx})_e = 15$ keV/nm as in Ref. [18], we employed the inelastic thermal spike model [17] in combination with MD to analyze the effect of energy transfer from the electronic subsystem to the lattice after the ion impact. In this model, the evolution of the electronic and lattice temperature is followed by solving simultaneously two differential equations:

$$C_e \frac{\partial T_e}{\partial t} = \frac{1}{r}\frac{\partial}{\partial r}\left[rK_e(T_e)\frac{\partial T_e}{\partial r}\right] - G\cdot(T_e - T_a) + A(r,t), \quad (1)$$

$$C_a \frac{\partial T_a}{\partial t} = \frac{1}{r}\frac{\partial}{\partial r}\left[rK_a(T_a)\frac{\partial T_a}{\partial r}\right] + G\cdot(T_e - T_a), \quad (2)$$

where r is the radial distance to the center of ion track and t is the time. Furthermore, C_e, C_a and K_e, K_a denote the heat capacity and thermal conductivity of the electronic and lattice subsystems, whereas G corresponds to the electron-phonon coupling, responsible for the energy exchange between electrons and lattice in the model. The term $A(r,t)$ represents the initial energy deposited after the ion-induced electron cascade; in our simulations we

employed the Waligorski distribution [36] re-fit to match the stopping power from the SRIM database [37] to obtain $A(r,t)$. We used the same electronic parameters for graphene as in [18], but with electronic thermal conductivity $K_e = 20.8\ Wm^{-1}K^{-1}$ instead. We employed graphite lattice parameters from [38, 39]. For a-C lattice, we used the same parametrization as in previous work [20] . For diamond, the electronic parameters were calculated as in [40], and the lattice ones were obtained from [38, 41]. The lattice thermal conductivity of graphite and diamond was reduced to $K_a = 1\ Wm^{-1}K^{-1}$ for temperatures higher than the melting point to take into account the amorphization of the material. The differential equations were solved independently for each material, assuming no energy exchange in the interface of the different materials. We solved the differential equations until most of the energy was transferred from the electrons to the lattice. We extracted the radial energy distribution in the lattice subsystem from the solver and we added it instantaneously to our atoms in the MD cell.

We simulated the SHI irradiation using adaptive timestep to cope efficiently with the radiation induced effects in materials. We employed the Berendsen thermostat at the borders of the cell to allow energy dissipation in the cell during irradiation. The border region was cooled to 300 K and the thickness of the border region was 5 Å along the x- and y-borders. The entire SHI irradiation process last for 100 ps to let the heat dissipate from the region of interest to the borders of the cell.

3. Results and discussion

3.1. Sputtering yield and track radius distribution

We analyzed the sputtering yield of graphene and track radius in three different structures at 100 ps after SHI irradiation, which all have the same size in xy-plane of 270×240 Å^2: suspended graphene, diamond supported graphene (as Figure 1), and sandwich structure consisting of DLC with different sp^3 fractions, graphene, and diamond (as Figure 2), respectively. The sputtering yield of suspended graphene is 90 atoms, and almost half of these atoms sputtered upwards while the other half went downwards. However, for the diamond-supported graphene, there were 39 atoms sputtered upwards with the same energy distribution while no atoms are sputtered from the bottom of diamond. Thus, the supporting diamond functioned as a shield that reflected all the downward sputtering atoms back to graphene layer. There were no sputtering atoms from graphene in the sandwich structures

because graphene is in the middle part and sputtered atoms were either absorbed by DLC or diamond, or reflected by them and stayed in graphene layers.

The way to determine the track radius in bulk materials, such as DLC and diamond, we used the format of Fermi function to fit sp^3 fraction in them along the radius direction, which can be expressed as [20, 42]:

$$y = \frac{A}{\exp(\frac{x-r_0}{t}) + 1} + C, \tag{3}$$

where A is the amplitude of sp^3 fraction, x radial position, r_0 track radius, t the width of transition area between the damaged and undamaged regions around the ion track, and C the constant. After fitting, the parameter r_0 with error bar was plotted as the track radius for DLC and diamond in Figures 3 and 4.

In 2D materials, such as graphene, the use of the same Fermi function to obtain track radius is inappropriate. Instead, we calculated the area of damaged region in each layer of graphene by observing the cross section through OVITO and then converted it to a circle that has the same area to get equivalent track radius in graphene layers. In Figure 3, we demonstrate how the track radii change through the sandwich structures in all three cases. Since the track morphology is overall very similar, we show only one exemplary image of the 70 eV DLC sandwich structure with the final track (Figure 3(d)). When comparing track radii in each layer separately, it is clear that track radius in DLC structure is much larger than that in diamond, also visually seen in Figure 3(d). We note here that in our structures we observe the track formation in diamond as well, but only at the top and the bottom of the diamond layer. Given that thermal conductivity plays a key role in Eqs. 1 and 2, it affects the final radial energy distribution in different materials. The higher the thermal conductivity of a material, the smaller the track radius will be formed in bulk materials. A disordered structure leads to reduction of thermal conductivity because of phonon scattering, which further leads to difficulties in heat diffusion from the center of the ion track. Nevertheless, the track radius in graphene is slightly larger than that in diamond though the thermal conductivity of graphene is much higher than in diamond. This can be attributed to the weak interlayer interaction in graphene, which makes it easier for carbon atoms to move away from the graphene layers and become sputtered atoms, colliding with others. For the same reason, track radius only shows up in the top and bottom surface of diamond.

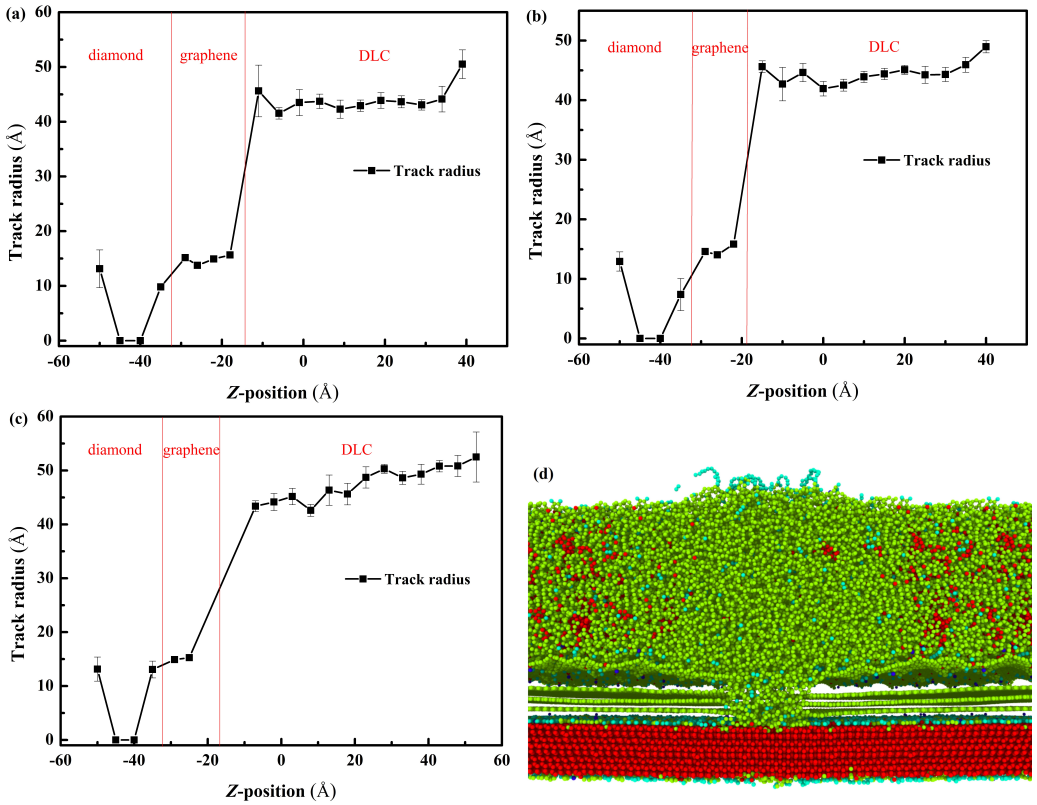

Figure 3: Track radius in sandwich structures with the deposited DLC under (a) 50 eV, (b) 70 eV, and (c) 100 eV as a function of z-position. (d) The cross section of the track image with atoms colored according to their coordination number: dark blue for 1, light blue for 2, green for 3, and red for 4.

To further investigate the protective properties of DLC films on multilayer graphene under it, several structures were simulated. They were similar to the above mentioned sandwich structure and of the same size in xy-plane, only replacing original graphene and deposited DLC with 6 layers of intact graphene and DLC with high sp^3 fraction (around 40%), as prepared by Kupka *et al.* in Ref. [20]. In addition, sandwich structures with diamond and low sp^3 fraction cover (15.45%) were also set for comparison, since both structures represent different covering situations. Figure 4(a) shows the track radius in different material combinations, and Figure 4(b) gives a closer look at track radius in graphene. Figure 4(a) reveals that track radius in diamond lies in the range between 10 to 15 Å in all cases similar to that in Figure

3, indicating that diamond was barely affected by the atoms sputtered from the graphene layers during SHI irradiation.

Comparison of the track radii in different DLC films in Figure 4(a) shows that DLC with low sp^3 content has smaller track radius than that of the higher sp^3 content DLC. Nonetheless, in Figure 3, the average track radius in DLC prepared under 100 eV condition, the lowest sp^3 content, is largest amongst the loose DLC structures prepared in this work. On one hand, the higher sp^3 content makes the DLC have more carbon atoms per unit volume, which increases the number of atoms excited initially at the center of the ion track, hence, effectively increasing the energy transfer to the lattice. On the other hand, lower sp^3 fraction endows DLC with lower thermal conductivity, leading to heat confinement near the center of the track for longer time, which would increases the probability of larger disorder due to local heating effects.

From Figure 4(b), we can conclude that track radius in all situations, except for diamond supported graphene, shows a similar trend with larger damaged area in outer layers while the track radius is reduced inside of the graphene. When graphene is covered by diamond on both sides, the diamond cover shrinks the track radius in one graphene layer at the position of 2 Å and expands the track radius in all other layers. For graphene layers covered by high sp^3 fraction DLC, the track radius increases considerably in graphene layer near DLC side while it decreases at 2 Å position too. In addition, the larger track radius in graphene appears at the DLC side, as shown in Figure 3.

The diamond and DLC cover once again play a role of reflective wall to prevent energetic atoms to sputter into surrounding environment and force them back towards graphene, leading to severer damage situation in graphene layers close to the reflective wall. Considering that diamond consists of pure sp^3 hybridized carbon atoms, the chemical bond is strong enough to avoid its own atoms to be sputtered during the SHI impact. Nevertheless, the DLC film has sp^2 carbon atoms dominating the whole structure, which can break easier than the sp^3 bond due to fewer σ bonds. When irradiated by SHI, these atoms at the bottom of DLC have much higher chances than those in diamond to become sputtered and shoot towards graphene and cause larger track radius. Due to higher atom density in DLC with higher sp^3 content, it will release more atoms to hit graphene when irradiated by SHI and broaden the track radius not only in DLC itself but also in the underneath graphene. Thus, we conclude that even though the high sp^3 content DLC film

can protect graphene from external force destruction, it may cause severer damage to the underneath graphene during SHI impacts.

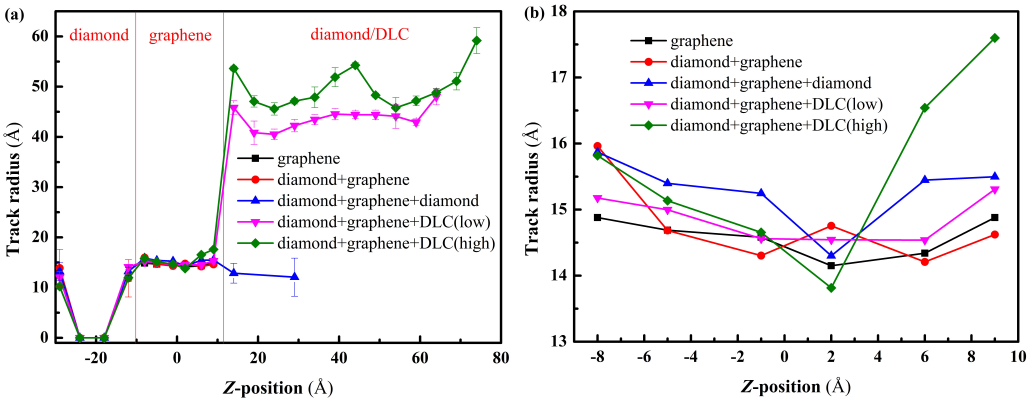

Figure 4: (a) Track radius in different combinations as a function of z-position and (b) partial enlargement of track radius in graphene.

3.2. Temperature, density, and sp^3 fraction distribution and evolution in DLC

As one of the key parameters to describe the heat dissipation during irradiation, the radial temperature distribution of carbon atoms in DLC with different sp^3 fractions was studied and plotted in Figure 5. Here we also display the temporal evolution of the temperature profile in the 70 eV DLC sandwich structure, since this parameters in the other two DLC structures behaved in the very similar manner. The temperature of carbon atoms around the ion tracks can be extremely high, even reaching over 11000 K, and then it dropped with the cooling rate decreasing with time. This observation is well in line with the results on temperature evolution in diamond and graphite reported in Refs. [43, 44].

Mass density spatial and temporal distributions in the DLC films are shown in Figure 6. The three subfigures show that the atomic density for all DLC films drops dramatically in the first 0.5 ps. At the core of the ion track, the density decreases to nearly 2.0 g/cm^3 as shown in Figure 6. The high temperature as shown in Figure 5 indicates high kinetic energies of the atoms which cause an immediate volume expansion, pushing the loose DLC structure outwards from the track. It is seen in a slight increase of densities at about 0.2 ps, the time which was sufficient enough for the lattice to respond

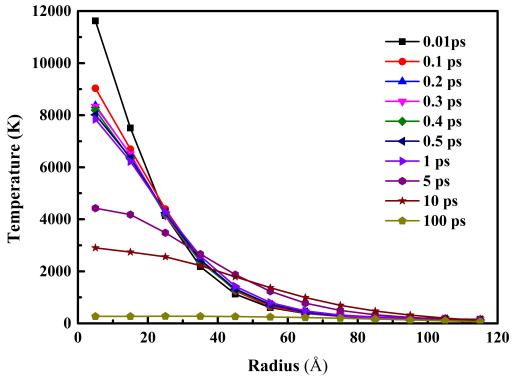

Figure 5: Radial temperature distribution of DLC deposited under 70 incident carbon atoms from SHI irradiation center at different time in the initial 100 ps right after start of irradiation.

to the swift energy deposition during the SHI impact. This overdense shell expands until 0.5 ps, when the density in the core of the track reaches its minimum value. After that, the overdense region starts relaxing returning the atoms back to the underdense core, smoothing the atomic density throughout the cell. However, the time is not sufficient to reach the full recovery of the density change and we observe the underdense track with the density $\rho_{tr} \approx 2.5$ g/cm^3 even after 100 ps of the track evolution, but no overdense shell, which is contrary to the core-shell structure of the tracks in, for instance, the SiO_2 as in Refs. [42, 45–47]. Similar decrease of the density in the center of the track was seen in Ref. [44], which agrees well with the present results. By this time, the entire system reaches the ambient temperature of 300 K. The described process is better observed for the DLC films of higher sp^3 content as shown in Figures 6(a) and 6(b). We also notice that the density in the entire cell becomes somewhat smaller than that of the original cell. It is clear that the number of atoms have been reduced by the electronic sputtering (since the top of the DLC film is an open surface). The denser the DLC film is, the higher the temperature is in the track core and, hence, the sputtering yield. In the poorest quality of the DLC concerning density (see Figure 6(c)), the decrease of the atomic density after the impact is the lowest. Eventually, in all the studied structures we measured the track radii $r_t = 45.08 \pm 0.66$ Å.

In Figure 7, we plotted the fraction of sp^3-hybridized carbon atoms binned radially from the center of the track for all the DLC films prepared in this

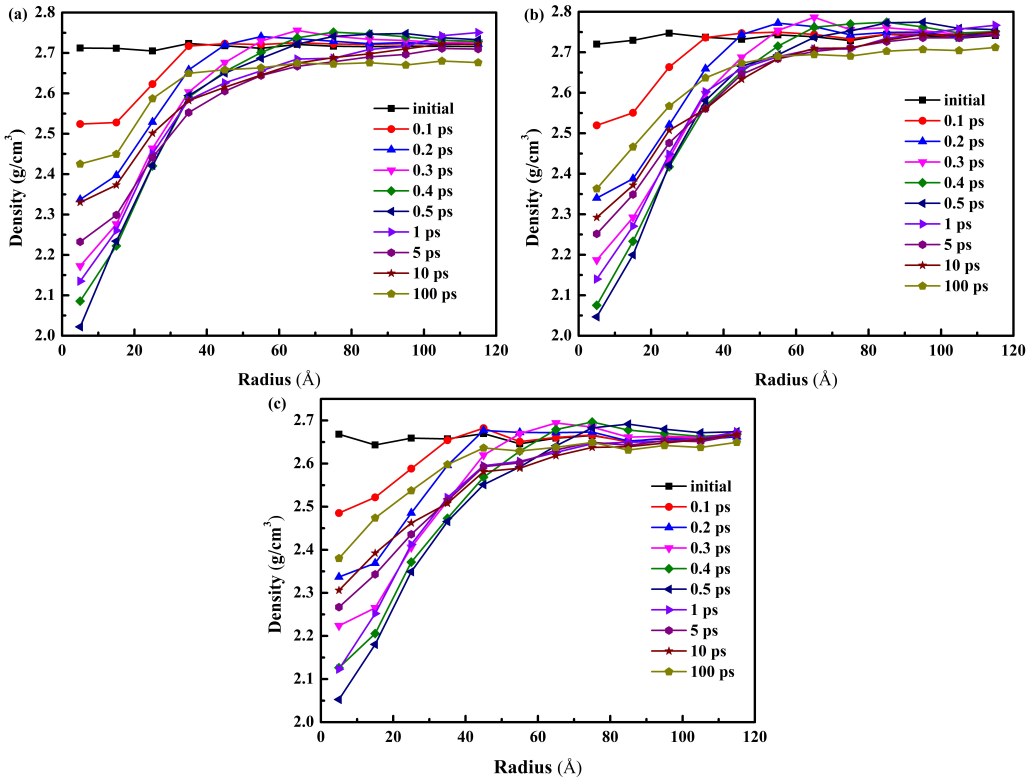

Figure 6: Radial density distribution of DLC deposited under (a) 50, (b) 70, and (c) 100 eV incident carbon atoms from SHI irradiation center at different time in the initial 100 ps right after start of irradiation.

work. Similar to Figure 6, there is a wide variation of this fraction within 70 Å radius range, beyond which almost all curves converge to the initial value. From the comparison of Figures 6 and 7, there is a clear correlation between the sp^3 content and the change of the atomic density. The higher the fraction of the sp^3 atoms the denser the structure of the material is. Thus, the diamond structure which consists of sp^3-bonded atoms is much denser than graphite with atoms bonded as sp^2.

The high pressure caused by very high temperatures in the core of the track increases the sp^3 fraction to over 20% at least until the first 0.1 ps, which is seen in Figure 7 as a strong peak for all cases. Already after 0.2 ps, it drops back to its original value in Figures 7(a) and (b)), while in the case with the DLC structure of the lowest sp^3 content (see Figure 7c), the original value is restored only after 0.3 ps. In this case, the peak value of the

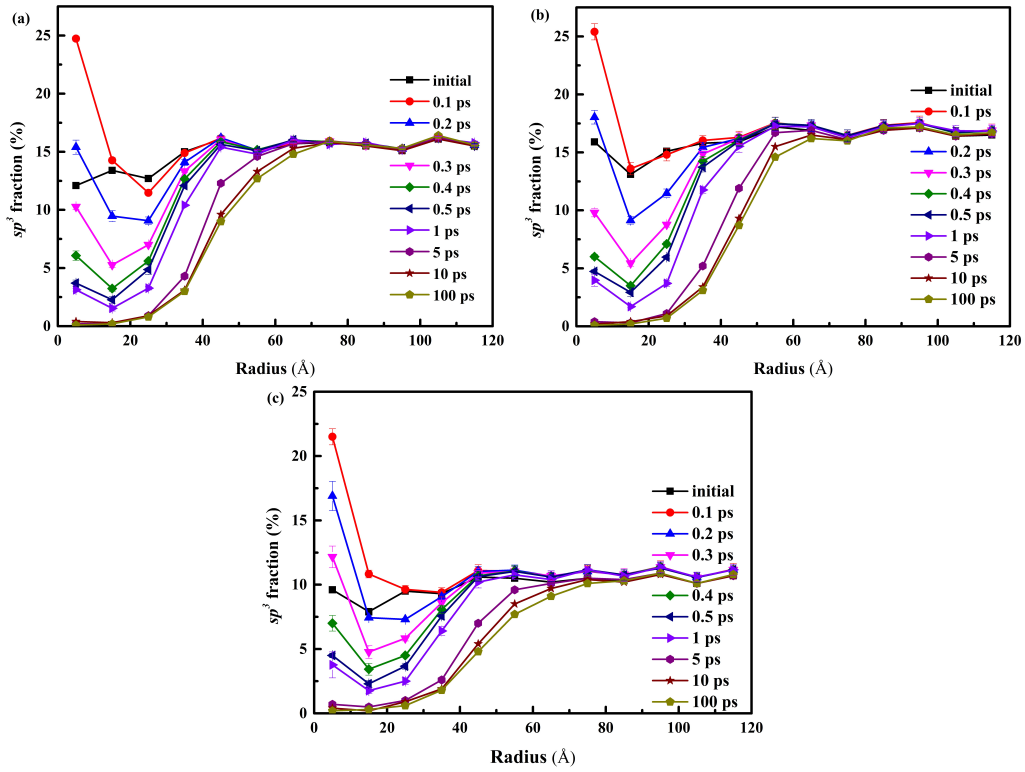

Figure 7: Radial sp^3 fraction distribution of DLC deposited under (a) 50, (b) 70, and (c) 100 eV incident carbon atoms from SHI irradiation center at different time in the initial 100 ps right after start of irradiation.

sp^3 fraction is in the middle of the ion track. From these results, we conclude that the high density of the deposited energy generates sufficient pressure to create more of the sp^3-bonded atoms at the core of the track. However, this is a transient process, as the thermal expansion exerts the pressure on the sides of the track reducing the local stress at the core of it and, eventually, the fraction of the sp^3-bonded atoms drops to zero within the track radius of 20 Å and does not change anymore until the end of the simulation. Similar observation was made in Ref. [48], where almost no sp^3 carbon atoms were found in the center of the track center, while the amount of sp^3 fraction dropped to half in the area around track center compared to the sp^3 fraction in the bulk. We note also that the sp^3 content recovers gradually to the bulk value within the track radius of almost 80 Å, while the atomic density recovers slightly faster within the radius $\leq$ 60 Å.

3.3. Ring analysis

To further investigate the modification of structural properties of the DLC films deposited on a multilayer graphene as prepared in this study, we carried out also the analysis of the primitive rings [49] in the structures before and after the irradiation. Figure 8 shows the normalized ring number distributions in three different DLC films deposited with different incident energies before and after the SHI irradiation. In Figures 8(a)-(c), it is evident that low-member rings do not practically exist in these structure and only starting from 5-member rings, the amount of the larger primitive rings become significant. The 6-member rings is common for a perfect graphene sp^2 and a diamond sp^3 structures, are also detected, although they are not dominant in the structure, whereas the high-member $(7-10)$ rings indicating the disorder of the amorphous carbon structure are more prominent and, hence, clearly seen in Figure 8(c). In addition, the 5-element rings are stabilized at around 8% or 9%. Usually, when simulated with Brenner potential, the maximum number of rings among different ring size is 6-member ring in very low density DLC like 2 g/cm^3. However, the DLC density in our work is around 2.7 g/cm^3, which shifts the maximum number peak to larger ring size, as shown in Marks' work [34]. Thus, according to this research, we produced a similar results of normalized ring number as a function of ring size.

The normalized ring number in different DLC at 1 ps after the ion impact is plotted in Figures 8(d)-(f). Although the time since the impact is rather short, the atomic dynamics affected the ring number distribution, *i.e.* the atom structure, and causes the huge fluctuation on that, especially within 40 Å from the center. In these figures, we detect the increase of the 3-member ring. The normalized number of these rings within the core of the track is 5 to 7 times higher than that in the remainder of the structure. For high-member rings (> 6) in Figures 8(d)-(f), there is a similar trend that the normalized ring number near the irradiation core fluctuates considerably compared to the one far away from the core. Thus, 10-member rings have a larger share than the 7-member rings in loose structure DLC in Figure 8(f), contrary to the denser DLC in Figures 8(d) and (e).

To check the long-term structure evolution, we also studied the normalized ring numbers at 100 ps in all studied DLC structures after SHI impact, which are shown in Figures 8(g)-(i). In these figures we also see a clear threshold that separates the affected and less affected regions in all cases. Unlike the ones in Figures 8(d)-(f), the threshold radius in Figures 8(g)-(i) is around 60 Å, within which there is a large change in the numbers of the

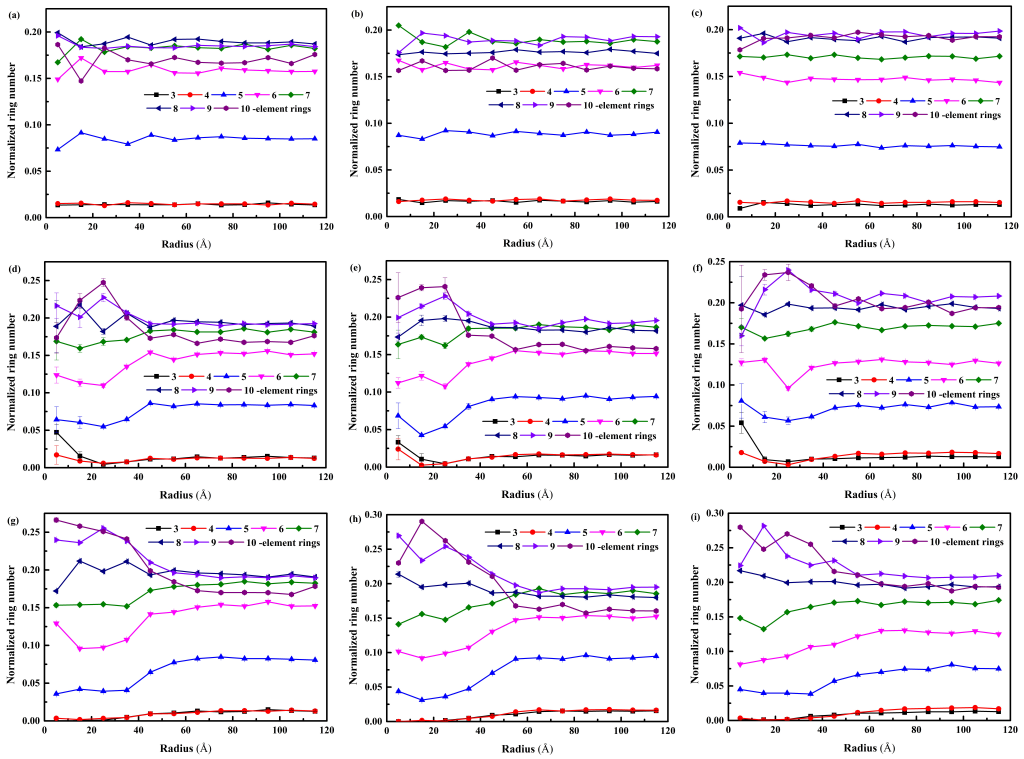

Figure 8: Normalized ring number distribution of DLC deposited under (a) (d) (g) 50, (b) (e) (h) 70, and (c) (f) (i) 100 eV incident carbon atoms. (a) (b) (c) are before SHI irradiation while (d) (e) (f) are 1 ps and (g) (h) (i) are 100 ps after SHI irradiation .

5- to 10-member rings as it is visible in Figures 8(g) and (h), and of the 9- and 10-member rings in Figure 8(i). In addition, the number of the 3- and 4-member rings dropped notably and is now even almost 0 within 40 Å. At the distance 15 – 55 Å, the normalized 5- and 10-member ring numbers differ the most substantially in Figures 8(g)-(i). It is worth noticing that 5- to 7-member ring number within 60 Å is smaller than it beyond this radius while 8- to 10-member ring number is larger. This can be inferred that SHI created a much more chaos area and eliminated sp^3 fractions within certain radius compared to the bulk region, although the bulk DLC itself is already disordered structure.

Comparison of the same DLC structure before and after SHI irradiation at different times reveals some interesting observations. For instance, the same rule for 3- and 4-member rings in all DLC structures is observed in

Figure 8(a) to Figure 8(g). Such a persistent ratio of all primitive rings in the system confirms that the effect of relaxation of the lattice after the ion impact is very short and no significant diffusion-type moves of atoms do not take place in these circumstances. The changes of numbers are clearly caused by the fast displacements resulting in changing the related rings (5- and 6-member rings exchange with the 8- to 10-member rings).

4. Conclusions

In this study, by utilizing the inelastic thermal spike model combined with molecular dynamics simulations, the structural modification of multi-layer graphene and protective DLC films due to SHI impact were studied. We found that the protective cover over graphene behaves as a reflective wall for carbon atoms sputtered through the electronic sputtering from graphene. In addition, the low thermal conductivity of DLC films causes heat confinement within the narrow track regions leading to strong internal electronic sputtering of atoms from the DLC film towards graphene. Thus, although high sp^3 fraction DLC film can serve as a good protective layer for multy-layer graphene from mechanical and external force destruction, it will cause severer damage to graphene under SHI irradiation. Analysis of the radial distribution of atomic density indicated formation of an ion track of 40 Å in radius, within which a low-density area with very low sp^3 content is forming. Interestingly, we observe a core-shell structure of ion tracks in DLC based on the analysis of primitive rings rather than the atomic densities. The latter is gradually reducing from the shell to the core, while the primitive rings show increase of large rings over the 5 and 6-member rings. It is evident that the fast dynamics of energy dissipation in carbon structures as well as high transient pressure in the shell due to high temperatures in the ion tracks does not allow the system relaxing in more equilibrium state and it remains heavily disorganized.

Acknowledgements

We acknowledge the support provided by China Scholarship Council (CSC) during the visit of J. L. to University of Helsinki. We also acknowledge grants of computer capacity from the IT Centre for Science in Finland, CSC and the Finnish Grid and Cloud Infrastructure (persistent identifier

urn:nbn:fi:research-infras-2016072533). This work is also supported by Postgraduate Research & Practice Innovation Program of Jiangsu Province (Grant No. SJCX18_0109) and the Fundamental Research Funds for the Central Universities (Grant No. NJ20150021 and No. NJ20170012). F.D. acknowledges the collaboration within the COST action Action TUMIEE (CA17126), supported by COST (European Cooperation in Science and Technology) and the IAEA Coordinated Research Project "Ion beam induced spatio-temporal structural evolution of materials: Accelerators for a new technology era (CRP F11020)." for useful discussions on damage in graphene.

References

[1] K. S. Novoselov, A. K. Geim, S. V. Morozov, D. Jiang, Y. Zhang, S. V. Dubonos, I. V. Grigorieva, A. A. Firsov, Electric field effect in atomically thin carbon films, Science 306 (2004) 666–669.

[2] C. Shan, H. Yang, J. Song, D. Han, A. Ivaska, L. Niu, Direct electrochemistry of glucose oxidase and biosensing for glucose based on graphene, Anal. Chem. 81 (2009) 2378–2382.

[3] F. Schedin, A. Geim, S. Morozov, E. Hill, P. Blake, M. Katsnelson, K. Novoselov, Detection of individual gas molecules adsorbed on graphene, Nat. Mater. 6 (2007) 652.

[4] L. Gomez De Arco, Y. Zhang, C. W. Schlenker, K. Ryu, M. E. Thompson, C. Zhou, Continuous, highly flexible, and transparent graphene films by chemical vapor deposition for organic photovoltaics, ACS Nano 4 (2010) 2865–2873.

[5] X. Wang, L. Zhi, K. Müllen, Transparent, conductive graphene electrodes for dye-sensitized solar cells, Nano Lett. 8 (2008) 323–327.

[6] X. Li, Y. Zhu, W. Cai, M. Borysiak, B. Han, D. Chen, R. D. Piner, L. Colombo, R. S. Ruoff, Transfer of large-area graphene films for high-performance transparent conductive electrodes, Nano Lett. 9 (2009) 4359–4363.

[7] I. Montero, L. Aguilera, M. E. Dávila, V. C. Nistor, L. A. González, L. Galán, D. Raboso, R. Ferritto, Secondary electron emission under electron bombardment from graphene nanoplatelets, Appl. Surf. Sci. 291 (2014) 74–77.

[8] J. Robertson, Properties of diamond-like carbon, Surf. Coat. Tech. 50 (1992) 185–203.

[9] A. Voevodin, M. Donley, J. Zabinski, Pulsed laser deposition of diamond-like carbon wear protective coatings: a review, Surf. Coat. Tech. 92 (1997) 42–49.

[10] C. Wei, J.-F. Yang, F.-C. Tai, The stress reduction effect by interlayer deposition or film thickness for diamond like carbon on rough surface, Diam. Relat. Mater. 19 (2010) 518–524.

[11] Y. J. Won, H. Ki, Effect of film gradient profile on adhesion strength, residual stress and effective hardness of functionally graded diamond-like carbon films, Appl. Surf. Sci. 311 (2014) 775–779.

[12] N. Klyui, A. Liptuga, V. Lozinskii, A. Lukyanov, A. Oksanich, V. Terban, Application of diamond-like carbon films to increase transmission of semi-insulating gaas crystals in the ir spectral range, Tech. Phys. Lett. 38 (2012) 609–612.

[13] K. Bewilogua, D. Hofmann, History of diamond-like carbon films—from first experiments to worldwide applications, Surf. Coat. Tech. 242 (2014) 214–225.

[14] D. Schwen, C. Ronning, H. Hofsäss, Field emission studies on swift heavy ion irradiated tetrahedral amorphous carbon, Diam. Relat. Mater. 13 (2004) 1032–1036.

[15] J. Zeng, H. Yao, S. Zhang, P. Zhai, J. Duan, Y. Sun, G. Li, J. Liu, Swift heavy ions induced irradiation effects in monolayer graphene and highly oriented pyrolytic graphite, Nucl. Instrum. Meth. B 330 (2014) 18–23.

[16] O. Ochedowski, K. Marinov, G. Wilbs, G. Keller, N. Scheuschner, D. Severin, M. Bender, J. Maultzsch, F. Tegude, M. Schleberger, Radiation hardness of graphene and mos2 field effect devices against swift heavy ion irradiation, J. Appl. Phys. 113 (2013) 214306.

[17] M. Toulemonde, J. Costantini, C. Dufour, A. Meftah, E. Paumier, F. Studer, Track creation in sio2 and bafe12o19 by swift heavy ions: a thermal spike description, Nucl. Instrum. Meth. B 116 (1996) 37–42.

[18] H. Vázquez, E. Åhlgren, O. Ochedowski, A. Leino, R. Mirzayev, R. Kozubek, H. Lebius, M. Karlušic, M. Jakšic, A. Krasheninnikov, et al., Creating nanoporous graphene with swift heavy ions, Carbon 114 (2017) 511–518.

[19] W. Ren, F. Djurabekova, K. Nordlund, Swift heavy ion effects on dlc-nanotube-diamond thin films, J. Phys. D Appl. Phys. 50 (2017) 355301.

[20] K. Kupka, A. Leino, W. Ren, H. Vázquez, E. Åhlgren, K. Nordlund, M. Tomut, C. Trautmann, P. Kluth, M. Toulemonde, et al., Graphitization of amorphous carbon by swift heavy ion impacts: Molecular dynamics simulation, Diam. Relat. Mater. 83 (2018) 134–140.

[21] J. Liu, H. Vázquez, K. Nordlund, F. Djurabekova, Structural properties of protective diamond-like-carbon thin films grown on multilayer graphene, Journal of Physics: Condensed Matter 31 (2019) 505703.

[22] P. De Andres, R. Ramírez, J. A. Vergés, Strong covalent bonding between two graphene layers, Physical Review B 77 (2008) 045403.

[23] Y. Baskin, L. Meyer, Lattice constants of graphite at low temperatures, Physical Review 100 (1955) 544.

[24] P. Delhaes, Graphite and precursors, CRC Press, 2014.

[25] W. Ren, A. Iyer, J. Koskinen, A. Kaskela, E. I. Kauppinen, K. Avchaciov, K. Nordlund, Conditions for forming composite carbon nanotube-diamond like carbon material that retain the good properties of both materials, Journal of Applied Physics 118 (2015) 194306.

[26] H. J. Berendsen, J. v. Postma, W. F. van Gunsteren, A. DiNola, J. Haak, Molecular dynamics with coupling to an external bath, J. Chem. Phys. 81 (1984) 3684–3690.

[27] K. Nordlund, M. Ghaly, R. Averback, M. Caturla, T. D. de La Rubia, J. Tarus, Defect production in collision cascades in elemental semiconductors and fcc metals, Phys. Rev. B 57 (1998) 7556.

[28] M. Ghaly, K. Nordlund, R. Averback, Molecular dynamics investigations of surface damage produced by kiloelectronvolt self-bombardment of solids, Philos. Mag. A 79 (1999) 795–820.

[29] D. W. Brenner, Empirical potential for hydrocarbons for use in simulating the chemical vapor deposition of diamond films, Phys. Rev. B 42 (1990) 9458.

[30] D. W. Brenner, Erratum: Empirical potential for hydrocarbons for use in simulating the chemical vapor deposition of diamond films, Phys. Rev. B 46 (1992) 1948.

[31] K. Beardmore, R. Smith, Empirical potentials for c-si-h systems with application to c60 interactions with si crystal surfaces, Philos. Mag. A 74 (1996) 1439–1466.

[32] H. Jäger, K. Albe, Molecular-dynamics simulations of steady-state growth of ion-deposited tetrahedral amorphous carbon films, J. Appl. Phys. 88 (2000) 1129–1135.

[33] C. de Tomas, I. Suarez-Martinez, N. A. Marks, Graphitization of amorphous carbons: A comparative study of interatomic potentials, Carbon 109 (2016) 681–693.

[34] N. Marks, N. Cooper, D. McKenzie, D. McCulloch, P. Bath, S. Russo, Comparison of density-functional, tight-binding, and empirical methods for the simulation of amorphous carbon, Physical Review B 65 (2002) 075411.

[35] A. Stukowski, Visualization and analysis of atomistic simulation data with ovito–the open visualization tool, Model. Simul. Mater. Sc. 18 (2009) 015012.

[36] M. Waligorski, R. Hamm, R. Katz, The radial distribution of dose around the path of a heavy ion in liquid water, Nucl. Tracks Rad. Meas. 11 (1986) 309–319.

[37] J. F. Ziegler, M. D. Ziegler, J. P. Biersack, Srim–the stopping and range of ions in matter (2010), Nucl. Instrum. Meth. B 268 (2010) 1818–1823.

[38] N. M. Ravindra, S. R. Marthi, A. Bañobre, Graphene, in: Radiative Properties of Semiconductors, 2053-2571, Morgan & Claypool Publishers, 2017, pp. 6–1 to 6–3.

[39] C. Uher, 4.3. 2 temperature dependence of thermal conductivity of graphite, in: Thermal Conductivity of Pure Metals and Alloys, Springer, 1991, pp. 430–439.

[40] M. Toulemonde, W. Assmann, C. Dufour, A. Meftah, C. Trautmann, Nanometric transformation of the matter by short and intense electronic excitation: Experimental data versus inelastic thermal spike model, Nucl. Instrum. Meth. B 277 (2012) 28–39.

[41] D. C. Harris, Development of Chemical-Vapor-Deposited Diamond for Infrared Optical Applications. Status Report and Summary of Properties, Technical Report, NAVAL AIR WARFARE CENTER WEAPONS DIV CHINA LAKE CA, 1994.

[42] A. Leino, S. Daraszewicz, O. H. Pakarinen, K. Nordlund, F. Djurabekova, Atomistic two-temperature modelling of ion track formation in silicon dioxide, EPL (Europhysics Letters) 110 (2015) 16004.

[43] D. Schwen, E. Bringa, Atomistic simulations of swift ion tracks in diamond and graphite, Nuclear Instruments and Methods in Physics Research Section B: Beam Interactions with Materials and Atoms 256 (2007) 187–192.

[44] F. Valencia, J. D. Mella, R. I. González, M. Kiwi, E. M. Bringa, Confinement effects in irradiation of nanocrystalline diamond, Carbon 93 (2015) 458–464.

[45] P. Kluth, C. Schnohr, O. H. Pakarinen, F. Djurabekova, D. Sprouster, R. Giulian, M. C. Ridgway, A. Byrne, C. Trautmann, D. Cookson, et al., Fine structure in swift heavy ion tracks in amorphous sio_2, Physical Review Letters 101 (2008) 175503.

[46] A. A. Leino, S. L. Daraszewicz, O. H. Pakarinen, F. Djurabekova, K. Nordlund, B. Afra, P. Kluth, Structural analysis of simulated swift heavy ion tracks in quartz, Nuclear Instruments and Methods in Physics Research Section B: Beam Interactions with Materials and Atoms 326 (2014) 289–292.

[47] O. H. Pakarinen, F. Djurabekova, K. Nordlund, P. Kluth, M. C. Ridgway, Molecular dynamics simulations of the structure of latent tracks

in quartz and amorphous sio_2, Nuclear Instruments and Methods in Physics Research Section B: Beam Interactions with Materials and Atoms 267 (2009) 1456–1459.

[48] D. Schwen, E. Bringa, J. Krauser, A. Weidinger, C. Trautmann, H. Hofsäss, Nano-hillock formation in diamond-like carbon induced by swift heavy projectiles in the electronic stopping regime: experiments and atomistic simulations, Applied Physics Letters 101 (2012) 113115.

[49] X. Yuan, A. Cormack, Efficient algorithm for primitive ring statistics in topological networks, Comp. Mater. Sci. 24 (2002) 343–360.